Journal of Power Sources 211 (2012) 119–128

Contents lists available at SciVerse ScienceDirect

Journal of Power Sources

journal homepage: www.elsevier.com/locate/jpowsour

An indicator of zinc morphology transition in flowing alkaline electrolyte

Yasumasa Ito*,[1], Xia Wei, Divyaraj Desai, Dan Steingart, Sanjoy Banerjee

The CUNY Energy Institute, Department of Chemical Engineering, City College of the City University of New York, 140th St, Convent Ave, Steinman Hall #314, NY 10031, USA

ARTICLE INFO

Article history:
Received 17 March 2012
Accepted 19 March 2012
Available online 7 April 2012

Keywords:
Zinc morphology
Flow battery
Current density
Zinc concentration
Substrate

ABSTRACT

Changes in electrodeposited zinc morphology were experimentally investigated in a flowing alkaline electrolyte. Deposition of zinc on flat sheets as well as on new mesh-type reduced-area current collectors was studied. Zincate concentration in the electrolyte, flow velocity, and current density was varied over a wide range. The results show that the ratio between the effective current density and the limiting current density (current density ratio) which is directly related to the zincate concentration at the electrode surface determines the zinc morphology. Zinc morphology is mossy and porous when the current density ratio is below 0.4, whereas it is a mixture of mossy and crystalline structures when it is between 0.4 and 0.9. Only when the current density ratio is above 0.9, does zinc deposition become just crystalline and compact. This finding holds for both flat sheet and mesh-type reduced-area current collectors.

1. Introduction

The efficient use of electrical energy to make use of excess night time generation capacity and intermittent renewable energy sources such as solar and wind is of great importance for both environmental and economical reasons. Large electrical energy storage systems based on long-life rechargeable batteries are essential for storing and stabilizing electricity supplies from such applications. Zinc-based rechargeable batteries are a most attractive electrical energy storage system due to zinc's low cost, abundant supply, non-toxicity, ambient temperature operation, safety, and scalability. However, zinc-based batteries have seen limited in use because of short cycle life. The capacity of most of metal-based batteries, including zinc-based, usually deteriorates within several hundred cycles, whereas several thousand cycles are needed for large electrical storage applications.

The capacity deterioration of zinc-anode batteries is primarily caused by internal short circuit due to non-uniform electrodeposition of zinc [1,2]. In conventional non-flowing zinc-anode batteries, the driving force of zincate transfer is only molecular diffusion causing a thick concentration boundary layer of zincate to form on the anode surface during charging. Therefore, the system is driven far from equilibrium and dendritic zinc deposits tend to appear [3,4]. Once there appear, dendrites grow progressively on repeated cycling since the current density at the tips is higher than at other locations, and it eventually reaches the cathode [2], shorting the battery.

Taking zincate mass transfer from diffusion control to convection control by flowing the electrolyte is a method to bring the system closer to the equilibrium and suppress non-uniformity of deposition. There are a number of research papers on zinc morphology in flowing electrolytes [2,5–13]. Ito et al. [2] carried out battery cycling experiments in flow-assisted zinc–nickel oxide batteries and achieved 1500 deep cycles. The system was reconditioned by a deep discharging that cleaned off all the deposited zinc every 15 cycles. In their experiment, zinc morphology appeared was mossy in all the experiments. On the other hand, it is known that zinc morphology changes with anodic current density. It is mossy or bulbous when the current density is low, whereas it is either compact or dendritic when the current density is high [5–7,11,13]. For example, Gallaway et al. [13] carried out microfluidic experiments and found that zinc morphology changes from mossy to compact and finally dendritic as the current density is increased. Though this transition in zinc morphology has been qualitatively known, a quantitative parameter to predict zinc morphology has not been reported.

In this work, we tested mesh-type anode current collectors were also tested as new reduced-area current collectors for simple zinc electrodeposition in addition to a conventional flat sheet current

* Corresponding author. Dept of Mechanical Science and Engineering, Nagoya University, Furo-cho, Chigusa-ku, Nagoya 464-8603, Japan. Tel./fax: +81 52 789 4488.
E-mail addresses: yito@nagoya-u.jp, yito@che.ccny.cuny.edu (Y. Ito).
[1] Tel.: +1 212 650 8136; fax: +1 212 650 6660.

0378-7753/$ – see front matter © 2012 Elsevier B.V. All rights reserved.
doi:10.1016/j.jpowsour.2012.03.056

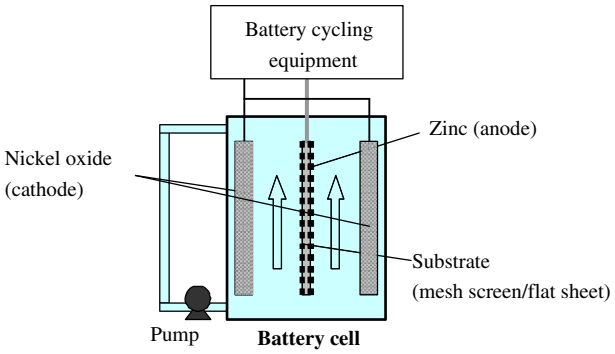

Fig. 1. Experimental setup.

collector. There are a few advantages of using reduced area of current collectors from a battery performance point of view. First, since zinc deposits not only on the surface facing to the cathodes but also in pores of the current collector, it should retard zinc approaching the cathode. Second, it enables increasing the effective current density only for anodes since the effective surface area for zinc deposition is small. This means that, for the cases where the optimal current density for the zinc anode is higher than that of the cathode, the efficiency of both electrodes and battery performance can be maximized by using a reduced-area current collector.

In this study, we aimed at finding a parameter which can quantitatively correlate the zinc morphology transition. Two types of expanded metal sheet were tested as reduced-area current collectors as anodes in zinc-anode batteries.

2. Experimental

Experiments have been carried out for zinc anode–nickel oxide cathode batteries. Fig. 1 shows the schematic of the experimental setup. The prismatic cell pack consisted of 2 positive and 1 negative plates alternately layered with a 3 mm gap. Metal zinc as negative (anode) electrode was deposited on a nickel-plated copper current collector. Two nickel-coated expanded copper sheets (DEXMET) were employed as reduced-area current collectors. Table 1 shows the specifications of the current collectors. Hereafter, the experiment using a flat sheet current collector is referenced as the "flat sheet" case, the 50% and 84% porosity expanded metal cases are referred as the "50%" and "84%" cases, respectively. A sintered nickel electrode (Jiangsu Highstar Battery Manufacturing) was used as the positive (cathode) electrode. Zinc oxide (Fisher Scientific ACS Grade) was initially dissolved into 45 wt% potassium hydroxide (KOH) solution (Fisher Scientific ACS Grade) as an electrolyte. The electrolyte flows from the bottom to the top of the battery. The electrolyte volume was carefully determined to keep the change of bulk zincate concentration less than 10% during cycling. Galvanostatic (constant current) battery cycling experiments were carried out using a battery cycle test equipment (Arbin BT2000). Table 2 shows the experimental conditions for zincate concentration, applied current density, and flow velocity, together with effective current density based on the surface area of the substrate. Charge capacity was set to 0.36 Ah based on the cathode capacity. The anode was taken out after the third charge, and zinc morphology was examined by a scanning electron microscopy (Hitachi TM3000). Furthermore, in order to investigate more detailed zinc structure, zinc anode was examined by using a 3D micro-computed tomography (μCT) (GE Healthcare Systems, London, ON, Canada). For this experiment, the electrodes were treated as follows to preserve the zinc structure. After rinsing in acetone, the electrode was dried in vacuum for 15 min. The dried sample was embedded in a spur low-viscosity media, consisting of ERL4221 (35.6 wt%), diglycidyl ether of polypropylene glycol (12.4 wt%), nonenyl succinic anhydride (51.2 wt%), and dimethylaminoethanol (0.9 wt%). Finally the sample was put in the oven at a temperature of 70 °C for about 8 h until the media hardened.

Table 1
Current collector.

Shape	Porosity [%]	Thickness [μm]	Effective surface area
Flat sheet	0	125	1
Expanded metal I	50	420	0.88
Expanded metal II	84	420	0.65

Table 2
Experimental conditions.

Test #	Current collector porosity [%]	Flow velocity [cm s^{-1}]	Zincate concentration [mol L^{-1}]	Applied current density [mA cm^{-2}]	Effective current density [mA cm^{-2}]
1	0	0.8	0.25	10.3	10.3
2	0	0.8	0.25	16.2	16.2
3	0	0.8	0.25	18.9	18.9
4	0	0.8	0.25	21.6	21.6
5	0	0.8	0.25	24.3	24.3
6	0	0.8	0.25	27.0	27.0
7	0	0.8	0.49	21.2	21.2
8	0	0.8	0.49	26.5	26.5
9	0	0.8	0.49	30.0	30.0
10	0	0.8	0.74	24.0	24.0
11	0	0.8	0.74	30.4	30.4
12	0	2.7	0.25	27.0	27.0
13	0	2.7	0.49	30.0	30.0
14	0	6.4	0.25	21.6	21.6
15	0	6.4	0.25	27.0	27.0
16	0	6.4	0.49	30.0	30.0
17	50	0.8	0.25	13.6	15.4
18	50	0.8	0.25	19.0	21.6
19	50	0.8	0.25	23.8	27.0
20	50	0.8	0.49	14.9	17.0
21	50	0.8	0.49	37.3	42.4
22	50	0.8	0.49	46.6	53.0
23	50	2.7	0.49	37.3	42.4
24	50	2.7	0.49	47.2	53.6
25	50	6.4	0.49	46.6	53.0
26	84	0.8	0.25	10.0	15.4
27	84	0.8	0.25	14.0	21.6
28	84	0.8	0.25	17.6	27.0
29	84	0.8	0.49	12.4	19.1
30	84	0.8	0.74	18.7	28.8
31	84	0.8	0.74	29.6	45.6
32	84	0.8	0.74	41.6	64.0
33	84	0.8	0.74	52.0	80.0
34	84	0.8	1.0	39.0	60.0
35	84	2.7	0.74	41.3	63.6
36	84	2.7	0.74	52.3	80.4
37	84	6.4	0.25	14.0	21.6
38	84	6.4	0.49	13.1	20.1
39	84	6.4	0.74	19.8	30.4
40	84	6.4	0.74	29.6	45.6
41	84	6.4	0.74	41.6	64.0
42	84	6.4	0.74	52.0	80.0
43	84	6.4	1.0	39.3	60.4

3. Results and discussion

Fig. 2 shows SEM images of zinc deposition at a zincate concentration of 0.25 mol L^{-1} and a flow velocity of 0.8 cm s^{-1}. It is found that when the current density is low, the structure is mossy and

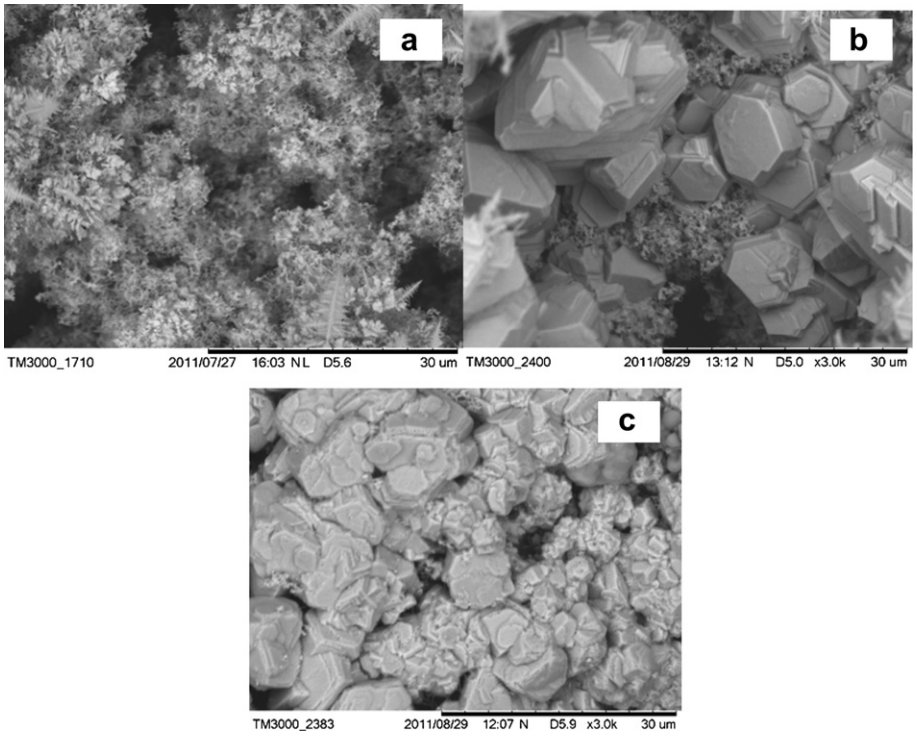

Fig. 2. Zinc morphology at various effective current densities at (a) 10.3 mA cm^{-2} (#1), (b) 21.6 mA cm^{-2} (#4), and (c) 27.0 mA cm^{-2} (#6).

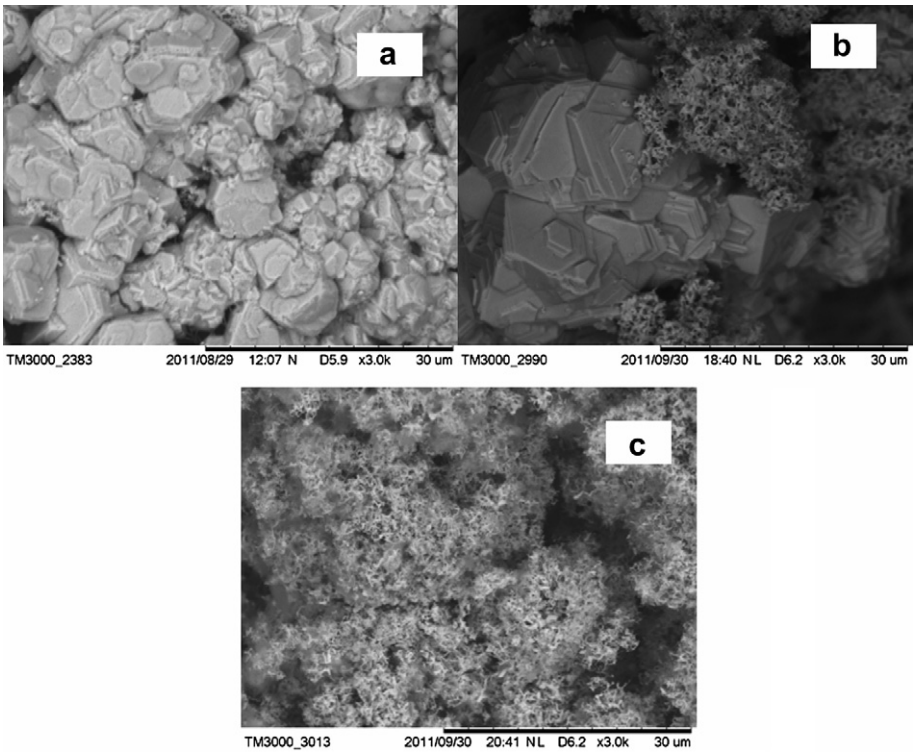

Fig. 3. Zinc morphology at zincate concentrations of (a) 0.25 mol L^{-1} (#6), (b) 0.49 mol L^{-1} (#8), and (c) 0.74 mol L^{-1} (#10).

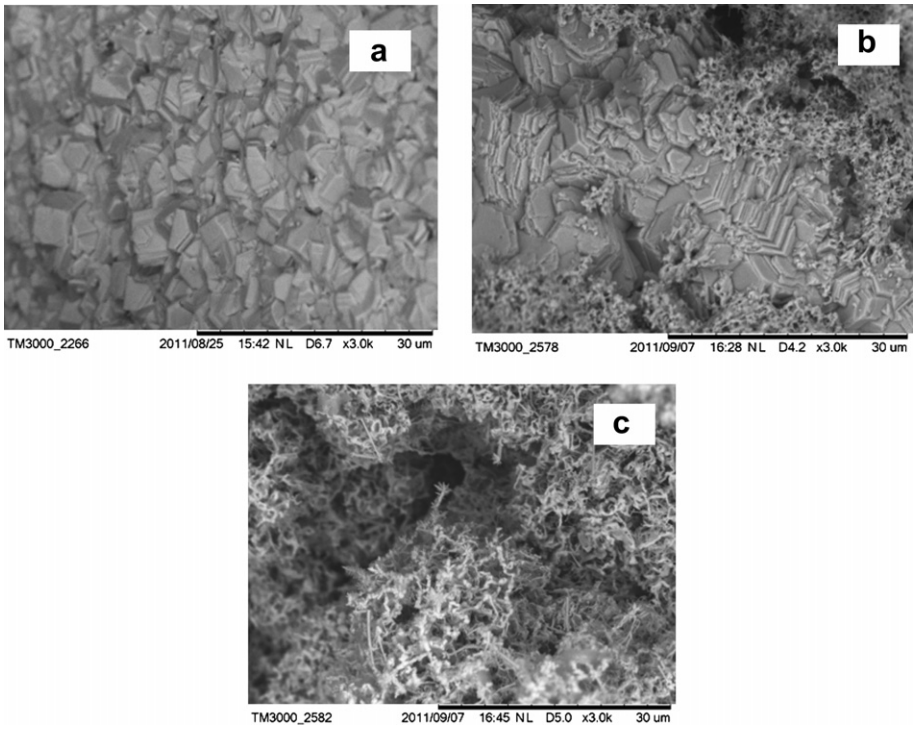

Fig. 4. Zinc morphology at flow velocities of (a) 0.8 cm s^{-1} (#33), (b) 2.7 cm s^{-1} (#35), and (c) 6.4 cm s^{-1} (#39).

Table 3
CD ratio of the experimental conditions.

Test #	Effective current density [mA cm^{-2}]	Limiting current density [mA cm^{-2}]	CD ratio
1	10.3	27	0.38
2	16.2	27	0.60
3	18.9	27	0.70
4	21.6	27	0.80
5	24.3	27	0.90
6	27.0	27	1.00
7	21.2	53	0.40
8	26.5	53	0.50
9	30.0	53	0.57
10	24.0	80	0.30
11	30.4	80	0.38
12	27.0	40	0.68
13	30.0	80	0.38
14	21.6	54	0.40
15	27.0	54	0.50
16	30.0	106	0.29
17	15.4	27	0.57
18	21.6	27	0.80
19	27.0	27	1.00
20	17.0	53	0.32
21	42.4	53	0.80
22	53.0	53	1.00
23	42.4	80	0.53
24	53.6	80	0.67
25	53.0	106	0.50
26	15.4	27	0.57
27	21.6	27	0.8
28	27.0	27	1.00
29	19.1	53	0.36
30	28.8	80	0.36
31	45.6	80	0.57
32	64.0	80	0.80
33	80.0	80	1.00
34	60.0	106	0.57
35	63.6	120	0.53
36	80.4	120	0.67
37	21.6	54	0.40
38	20.1	106	0.19
39	30.4	160	0.19
40	45.6	160	0.29
41	64.0	160	0.40
42	80.0	160	0.50
43	60.4	212	0.29

porous, whereas it shows compact and crystalline hexagonal structure when the current density is high. In the intermediate region, the structure is the mixture of mossy and compact structures. However, as shown in Fig. 3, zinc morphology change is obviously also a function of zincate concentration. The structure is still mossy at high current densities for high zincate concentration cases. Fig. 4 illustrates the effects of flow velocity on zinc morphology. Mossy structure appears as the flow velocity is increased.

All of these parameters change the distance of the system from equilibrium. The system becomes far from equilibrium with higher applied current density, lower bulk concentration of zincate, and slower flow velocity of the electrolyte, and the zinc morphology transients from mossy to compact accordingly, as shown in Figs. 2–4. Considering the limiting current density incorporates all of these factors, the ratio between the effective current density and the limiting current density,

$$\text{Current Density (CD) ratio} = \text{the effective current density} / \text{the limiting current density}$$

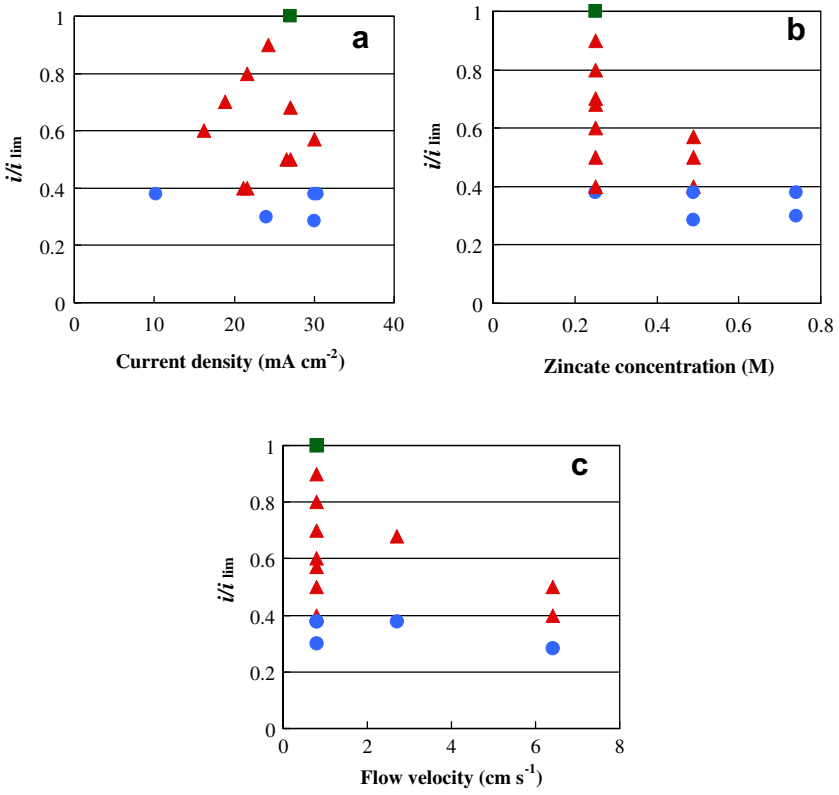

Fig. 5. Zinc morphology mapped by the CD ratio and (a) the current density, (b) zincate concentration, and (c) flow velocity for the flat sheet case (●: mossy, ▲: mossy and compact, ■: compact).

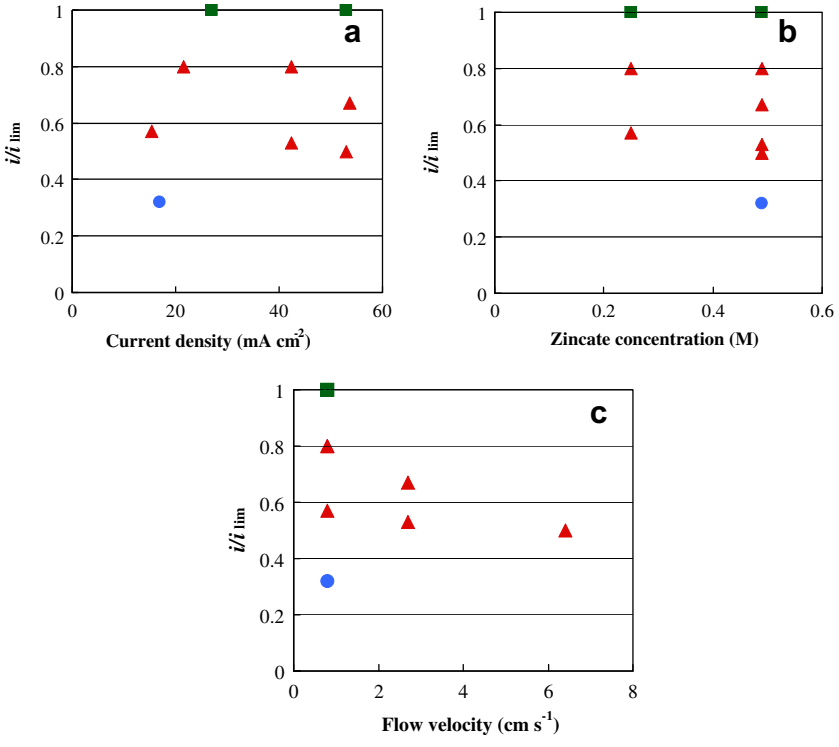

Fig. 6. Zinc morphology mapped by the CD ratio and (a) the current density, (b) zincate concentration, and (c) flow velocity for the 50% mesh case. Plots as in Fig. 5.

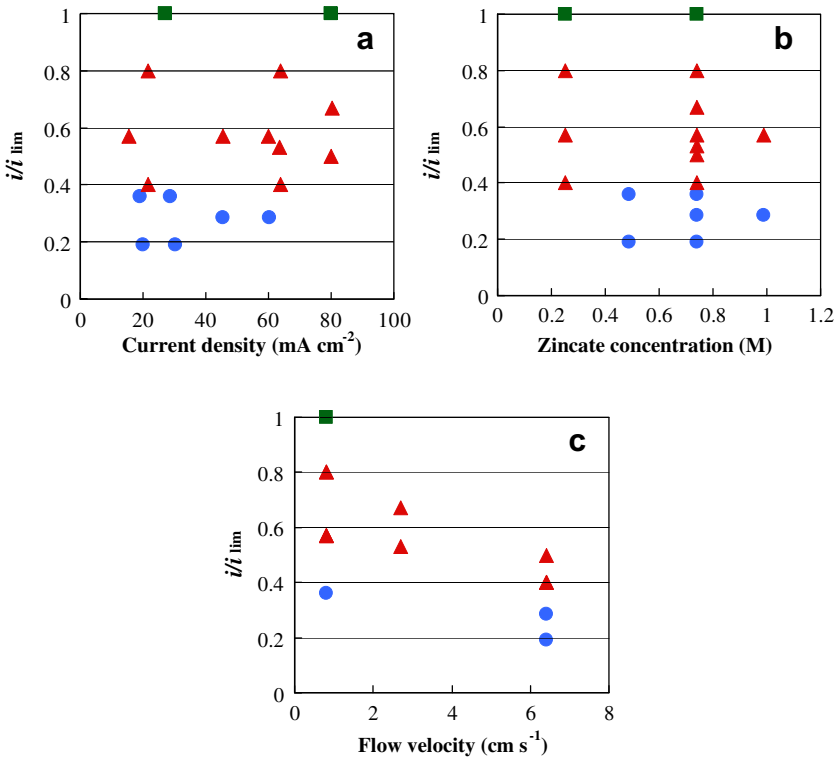

Fig. 7. Zinc morphology mapped by the CD ratio and (a) the current density, (b) zincate concentration, and (c) flow velocity for the 84% mesh case. Plots as in Fig. 5.

is tested as a measure which indicates the distance from equilibrium in this study. In our configuration, the limiting current density is given by Ref. [14]

$$i_{\mathrm{lim}} = \frac{nFDC_0}{d_{\mathrm{e}}}Sh \tag{1}$$

$$Sh = 1.85Re^{1/3}Sc^{1/3}(d_{\mathrm{e}}/L)^{1/3} \tag{2}$$

where i_{lim} is the limiting current density, n is the number of electron in the reaction, F is Faraday's constant, D is the diffusion constant, C_0 is the bulk zinc concentration, Sh is Sherwood number, Re is Reynolds number, Sc is Schmidt number, d_{e} is the hydraulic diameter, L is the plate length in the streamwise direction. On the other hand, the current density is described as follows [14];

$$i = i_0\left[\exp(\alpha_{\mathrm{a}}nF\eta/RT) - \left(\frac{C_{\mathrm{S}}}{C_0}\right)\exp(-(1-\alpha_{\mathrm{c}})nF\eta/RT)\right] \tag{3}$$

$$i = i_0\left[\exp(\alpha_{\mathrm{a}}nF\eta/RT) - \left(1-\frac{i}{i_{\mathrm{lim}}}\right)\exp(-(1-\alpha_{\mathrm{c}})nF\eta/RT)\right] \tag{4}$$

where i_0 is the exchange current density, C_{S} is the zinc concentration at the surface, R is the gas constant, T is the temperature. Therefore, i/i_{lim}, the CD ratio, indirectly means the zincate concentration at the anode surface. The CD ratio of the experimental conditions is shown in Table 3.

Figs. 5–7 show zinc morphology mapped by the CD ratio and (a) the current density, (b) zincate concentration, and (c) flow velocity, for the flat sheet, 50% mesh, and 84% mesh cases, respectively. The morphology is clearly categorized by the CD ratio regardless the current density, zincate concentration, flow velocity, and the substrates. When the CD ratio is less than 0.4, the morphology is just mossy and it becomes a mix of mossy and compact structures when 0.4 < CD ratio < 0.9. Completely compact structure appears only when the CD ratio is above 0.9. As summary, the representative images of zinc morphology at constant CD ratios in different experimental conditions and at the CD ratio of 0.3, 0.4, 0.6, 0.8, 0.9, and 1.0 are shown in Figs. 8 and 9, respectively. It is seen in Fig. 8 that the morphology is consistent at a constant CD ratio. On the other hand, Fig. 9 clearly shows the transition of morphology from mossy to compact as with increasing the CD ratio.

Fig. 10 shows the zinc morphology map against overpotential. Overpotential does not work as a quantitatively indicator for the morphology transition, since it is affected by the unrelated processes of kinetic activation and electrolyte resistance. The exchange current density also changes depending on the unrelated phenomena. In fact, as seen in Eq. (4), overpotential is basically independent from the term which involves the limiting current.

4. 3D micro computer tomography (μCT) of zinc anodes

The zinc anode was scanned on a μCT system to investigate the detailed structure. A filter at a wavelength of 10.5 nm was applied to separate non-zinc signals. Scanned images were reconstructed using a commercially available voxel analysis software package (MicroView, Version 2.2, GE Healthcare). Fig. 11 shows the reconstructed zinc image at various CD ratio. It was reconstructed with a voxel size of 9 μm. Porosity was calculated based on the reconstructed 3D images. The results are shown in Table 4. Note that since the deposition is dependent on the current collectors shape macroscopically, a portion which does not include substrate effects was selected in the calculation to exclude the effects. It is clearly observed in Fig. 11 that the deposition becomes more compact with increasing CD ratio, and it is quantitatively shown in Table 4.

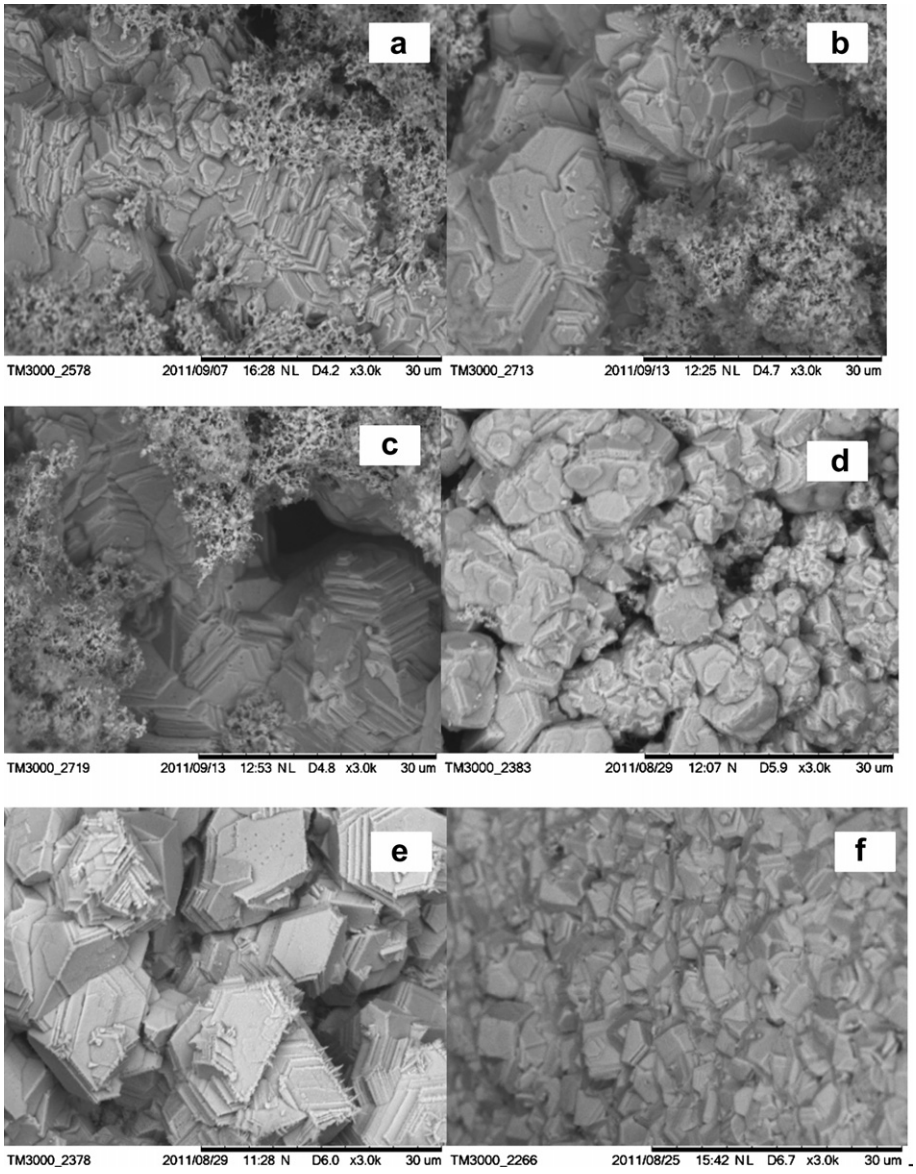

Fig. 8. Zinc morphology at the CD ratio of 0.5 ((a)–(c)) and 1.0 ((d)–(f)). (a) #15, (b) #25, (c) #42, (d) #6, (e) #22, and (f) #33.

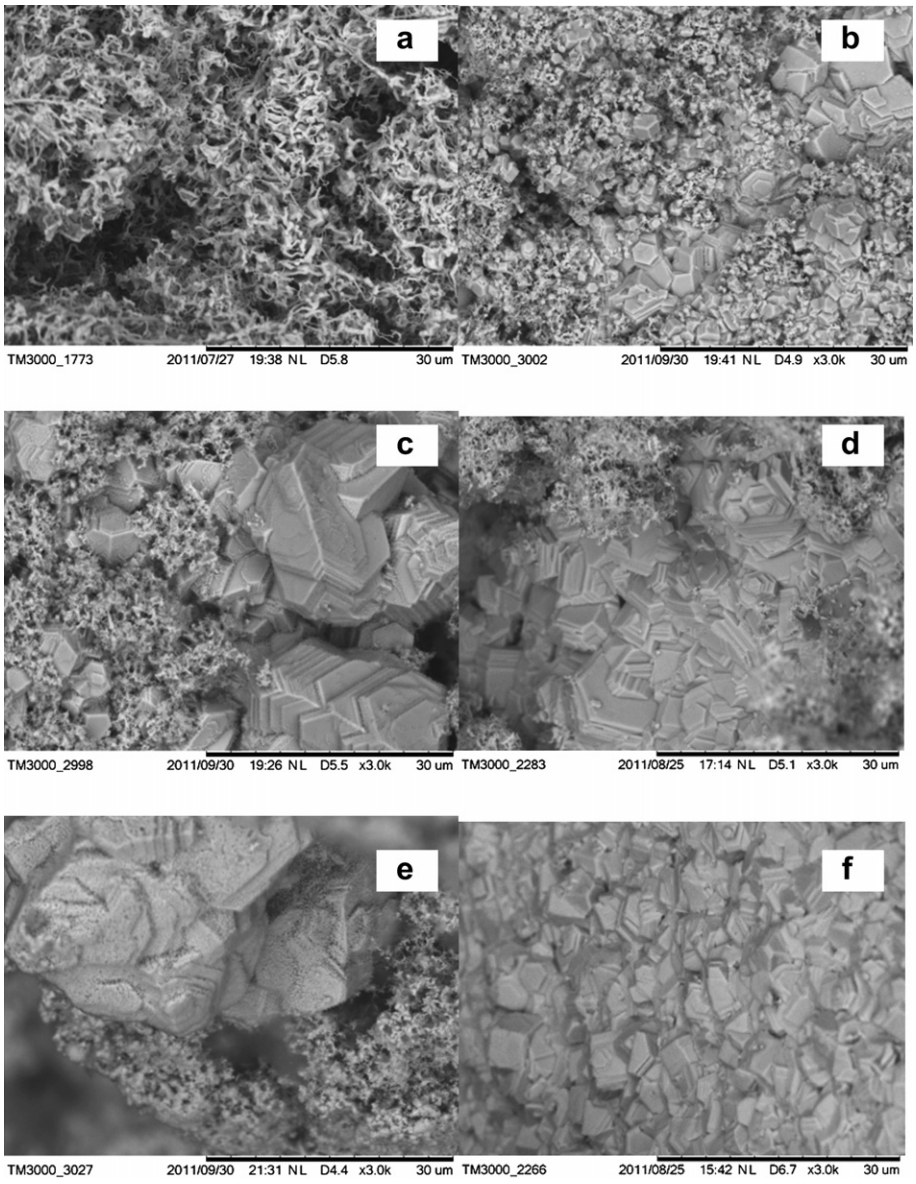

Fig. 9. Zinc morphology at the CD ratio of (a) 0.3 (#10), (b) 0.4 (#7), (c) 0.6 (#2), (d) 0.8 (#32), (e) 0.9 (#5), and (f) 1.0 (#33).

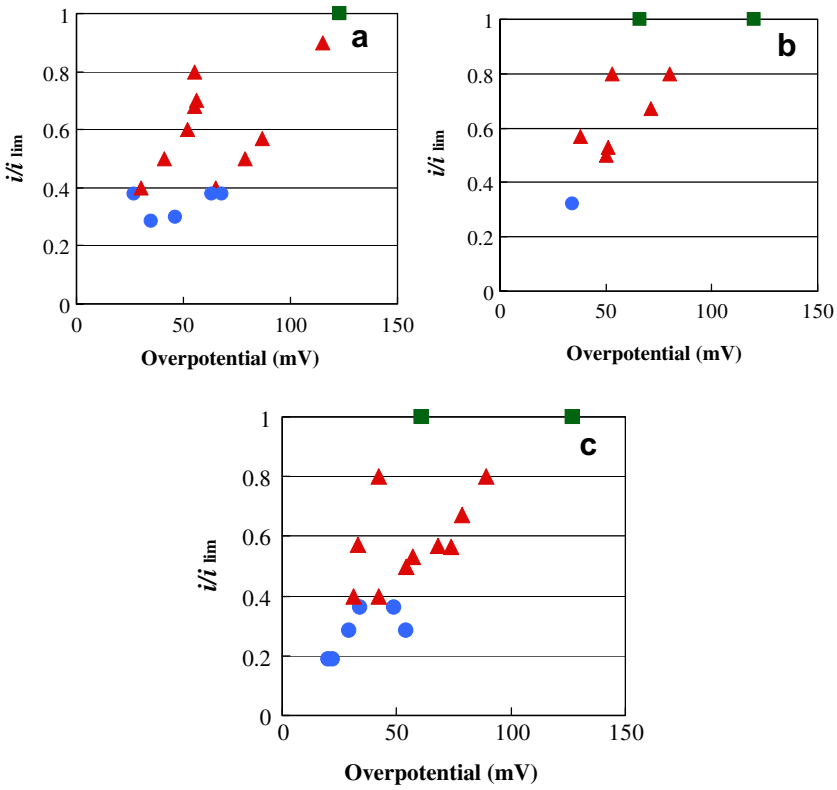

Fig. 10. Zinc morphology mapped by the overpotential. (a) Flat sheet case, (b) 50% mesh case, (c) 84% mesh case. Plots as in Fig. 5.

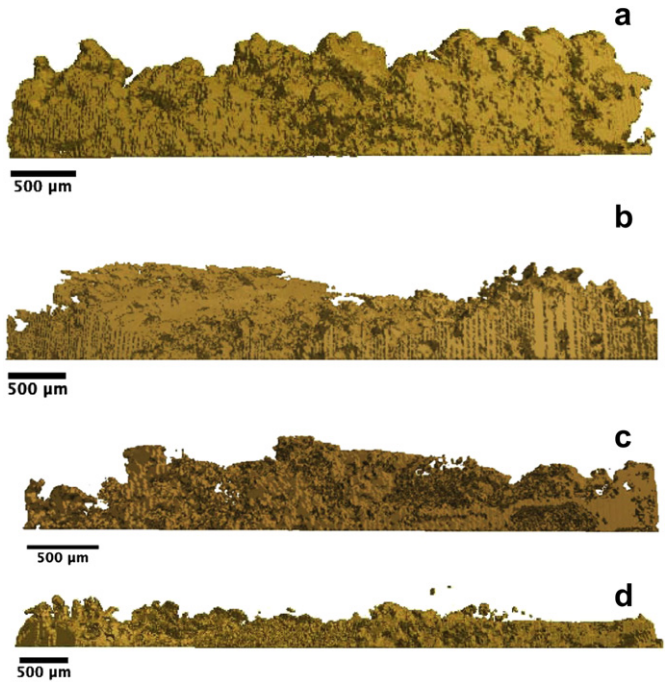

Fig. 11. 3D reconstructed images of zinc by the micro CT at a CD ratio of (a) 0.36 (#30), (b) 0.57 (#26), (c) 0.8 (#21), and (d) 1 (#33).

Table 4
Porosity of zinc.

CD ratio	0.36	0.57	0.8	1
Porosity	75.4	69.0	60.6	45.9

5. Conclusions

Zinc morphology transition in a flowing alkaline electrolyte was experimentally investigated. The study is summarized as follows.

1. The zincate concentration at the surface of the anode or the ratio between the effective current density against the limiting current density determines the zinc morphology.
2. Zinc morphology is mossy and porous when the current density ratio is below 0.4, whereas it is a mixture of mossy and compact structures when it is between 0.4 and 0.9. When the current density ratio is above 0.9, zinc deposition is compact.
3. The above findings apply for both a flat sheet and mesh-type reduced-area current collectors.
4. Zinc porosity decreases as the morphology changes from mossy to compact.

The current density ratio would enable us to predict zinc morphology in zinc-based batteries. Also it is shown that a reduced-area current collector such as an expanded metal modifies zinc electrodeposition. For example, in the case that only mossy and porous zinc appears at a given battery charge rate, as mentioned in Ito et al. [2], the effective current density at the anode can be increased by use of an reduce-area current collector to achieve compact zinc deposition. Furthermore, this study also pertains to pulse charging protocols. Pulse charging [15,16] is a well known method to achieve compact zinc deposition in non-flowing zinc-anode batteries. However, the protocols have been mostly empirically developed. On the other hand, this study

result allows direct calculation of the optimal values for parameters such as charging current density and durations for charge and rest.

Acknowledgements

The authors would like to show their gratitude to Prof. Cardoso (Dept. Biomedical Engineering, City College of New York) for the micro CT capability. We also appreciate Dr. Damon Turney (The CUNY Energy Institute, City College of New York) for useful discussion and comments on this manuscript and Dr. Joshua Gallaway (The CUNY Energy Institute, City College of New York) for his comments.

This work was performed under grants from National Energy Technology Laboratory (NETL) (#DE-EE0004224) and New York State Energy Research and Development Authority (NYSERDA) (#18786).

References

[1] D. Linden, T.B. Reddy (Eds.), Handbook of Batteries, third ed. (2001).
[2] Y. Ito, M. Nyce, R. Plivelich, M. Klein, D. Steingart, S. Banerjee, J. Power Sources 196 (2011) 2340.
[3] M. Minakshi, D. Appadoo, D.E. Martinb, Electrochem. Solid-State Lett. 13 (2010) A77.
[4] C. Cachet, B. Saidani, R. Wiart, J. Electrochem. Soc. 138 (1991) 678.
[5] R.D. Naybour, J. Electrochem. Soc. 116 (1969) 520.
[6] D.P. Sutija, R.H. Muller, C.W. Tobias, J. Electrochem. Soc. 141 (1994) 1477.
[7] J. Jorne, M.G. Lee, J. Electrochem. Soc. 143 (1996) 865.
[8] R.Y. Wang, D.W. Kirk, G.X. Zhang, J. Electrochem. Soc. 153 (2006) C357.
[9] Frank R. McLarnon, Elton J. Cairns, J. Electrochem. Soc. 138 (2) (1991).
[10] R.G.A. Wills, J. Collins, D. Stratton-Campbell, T.J. Low, D. Pletcher, F.C. Walsh, J. Appl. Electrochem. 40 (2010) 955.
[11] J. Cheng, L. Zhang, Y.S. Yang, Electrochem. Commun. 9 (2007) 2639.
[12] L. Zhang, J. Cheng, Y.S. Yang, J. Power Sources 179 (2008) 381.
[13] J.W. Gallaway, D. Desai, A. Gaikwad, C. Corredor, S. Banerjee, D. Steingart, J. Electrochem. Soc. 157 (2010) A1279.
[14] J. Newman, Electrochemical Systems, third ed., 2004.
[15] G. Bronoel, A. Millot, N. Tassin, J. Power Sources 34 (1991) 243.
[16] M.V. Simicic, K.I. Popov, N.V. Krstajic, J. Electroanal. Chem. 484 (2000) 18.